International Journal of Computational Methods
Vol. 12, No. 4 (2015) 1540012 (17 pages)

DOI: 10.1142/S0219876215400125

Special Elements for Composites Containing Hexagonal and Circular Fibers

Qing H. Qin* and H. Wang†

Department of Engineering Mechanics
Henan University of Technology
Zhengzhou, 450001, P. R. China
**qinghua.qin@anu.edu.au*
†huiwang_china@163.com

Received 9 September 2014
Revised 3 December 2014
Accepted 27 December 2014
Published 5 May 2015

In this paper, unidirectional fiber reinforced composites with periodic square array of circular and hexagonal fibers is studied by a novel fundamental-solution-based hybrid finite element model. Due to the periodicity of composites, a representative unit cell containing a single fiber with circular or hexagonal cross section is taken into consideration and analyzed using the proposed hybrid finite element model. In the present numerical model, special polygonal fiber elements with arbitrary number of sides are developed by coupling the independent element interior and frame displacement fields. The element interior displacement fields are approximated by the combination of fundamental solutions to prior satisfy the governing equation of the problem, so that the domain integral appeared in the weak-form hybrid functional in terms of dual variables is converted into boundary integrals. Independently the element frame displacement fields are approximated by the conventional shape functions to guarantee the continuity of adjacent elements. Following this, special polygonal fiber elements are constructed to reduce mesh effort in the fiber region and achieve good accuracy with fewer elements. Finally, numerical tests are carried out for assessing the performance of the present special elements.

Keywords: Periodic fiber reinforced composites; hybrid finite element method; fundamental solutions; special polygonal fiber element.

1. Introduction

In the context of composite with reinforced fiber inclusions, the simplified model with periodic distribution of multiple inclusions is usually taken as an example for determining the corresponding effective properties of composites. However, the

*Corresponding authors.

analytical methods like Fast Fourier transform-based method and so on [Yu and Qin (1996); Feng *et al.* (2003); Bonnet (2007); To *et al.* (2013)], are usually difficult to deal with composites containing inclusions with complicated geometric shapes or distributions. As alternatives to the analytical methods, numerical methods were developed for effectively solving such problems. For example, Würkner *et al.* [2011] evaluated effective material properties for composite structures with rhombic fiber arrangements by the finite element method (FEM). Michel *et al.* [1999] compared the two numerical methods including the FEM and the fast Fourier transform-based numerical method in determining effective properties of composite materials with periodic microstructure. Qin and Yang [2008] studied the effect of fiber bundling on the effective transverse properties of unidirectional fiber composites by way of the FEM. As one of numerical methods different to the FEM (a typical domain-discretizing method), the boundary element method (BEM) which employs fundamental solutions to fulfill the boundary discretization of the domain of interest was also carried out for analysis of periodic composites with fibers. For instance, Dong [2006] established a boundary element formulation for predicting the effective elastic properties of composites including doubly periodic array of inclusions. Yang and Qin [2004] extended the BEM to the micro-mechanical analysis of composite materials. Kaminski [1999] employed the boundary element formulations-based homogenization to deal with the periodic transversely isotropic linear elastic fiber-reinforced composites. Besides, Maxwell's methodology was combined with the complex-variable BEM for evaluating the two-dimensional effective elastic properties of composites with periodic or random fibers, pores, or cracks, provided that the overall behavior is isotropic, and inclusions'effects are assumed to be the same as those of an equivalent circular inhomogeneity [Mogilevskaya and Crouch (2013)].

Unlike the works mentioned above, Wang *et al.* [2011b] developed a hybrid finite element formulation based on fundamental solutions (named as HFS-FEM) for analyzing the thermal behavior of fiber-reinforced composites, in which the fiber can be regularly or randomly distributed. In the developed hybrid FEM, fundamental solutions satisfying the governing equation of problems or specific boundary conditions were used to approximate the element interior fields and thus the present method has shown some advantages over the FEM and the BEM [Qin and Wang (2008); Wang and Qin (2009)]. One feature of the present method is the use of special elements including the special hole element [Wang and Qin (2011a); Qin and Wang (2013)], special circular inclusion element [Wang and Qin (2011b)], special point-load element [Wang and Qin (2012)] and special graded element [Wang *et al.* (2012)]. In addition to the development of special elements based on the special fundamental solutions, another feature of the present hybrid finite element model is to construct arbitrarily shaped elements. In the algorithm, the frame fields defined along the element boundary is independent of the element interior fields which satisfy the governing equation and can convert domain integrals in the double-variable hybrid functional into element boundary integrals. Thus, all integrals appearing in the hybrid model are boundary integrals along the element frame. This means that you can arbitrarily design the number of edges and nodes of element according to your requirement. This feature was also found in other unconventional elements like the Trefftz elements [Qin (2000); Qin and Wang (2008)] and the Voronoi cell finite elements [Ghosh (2011)]. The former used Trefftz solution set to approximate the interior fields and the latter employed Airy's stress functions in terms of high-order polynomial expansion to approximate the interior stress field.

In this work, the HFS-FEM with special polygonal fiber elements is developed for unidirectional composites with doubly periodic polygonal fibers. In the present algorithm, special polygonal fiber elements with more than four edges and nodes are constructed by using two-dimensional plane strain fundamental solutions for solving elastic problems of composites to effectively reduce mesh density in the fiber region. For simplicity, only circular and hexagonal fibers are considered in this paper.

2. Computational Model

Consider an unidirectional composite with doubly periodic polygonal inclusions of arbitrary shape in a plane matrix (see Fig. 1). The elastic parameters of inclusion and matrix are respectively denoted by $E^{(\mathrm{I})}$ and $v^{(\mathrm{I})}$, and $E^{(\mathrm{M})}$ and $v^{(\mathrm{M})}$.

For such periodic structures, a representative rectangular unit cell shown in Fig. 1 with edge length of $2l$ and $2h$ along the coordinate directions x_1 and x_2 are chosen as an example. On the outer boundary of the unit cell, the suitable periodic boundary conditions corresponding to remote tension along x_1- and x_2-directions are given by [Dong (2006)]

$$\begin{aligned} u_1(l, x_2) &= -u_1(-l, x_2) = u_{l1}, \\ t_2(l, x_2) &= t_2(-l, x_2) = 0, \\ u_2(x_1, h) &= -u_2(x_1, -h) = u_{h2}, \\ t_1(x_1, h) &= t_1(x_1, -h) = 0, \end{aligned} \tag{1}$$

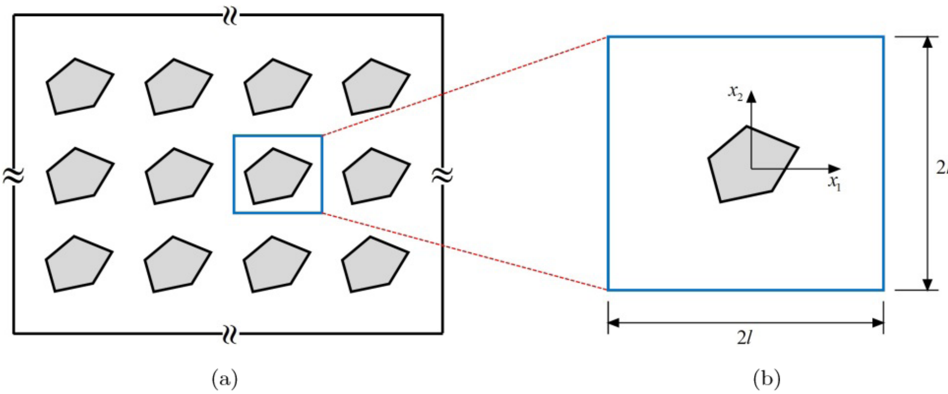

Fig. 1. Sketch of doubly periodic fibers with arbitrary shape in the infinite plane matrix and a rectangular unit cell. (a) Periodic composites and (b) unit cell.

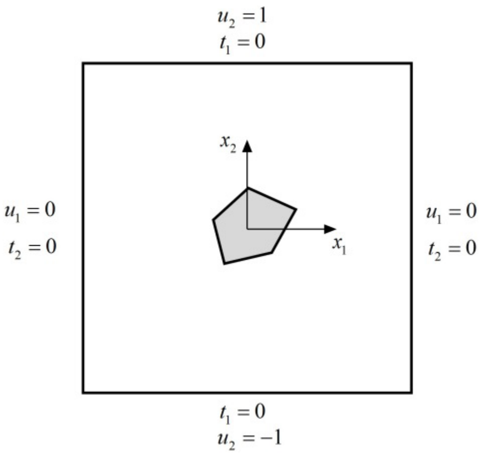

Fig. 2. Periodic unit displacement boundary conditions for the case of x_2-directional tension.

where u_{l1} and u_{h2} are specified constant displacements to keep the edges of the cell still to be straight after deformation.

For simplicity, only the square package is considered, that is $l = h$. Simultaneously, only the sub-model related to the x_2-directional unit tension (see Dong [2006]) is considered to show the efficiency of the present method. The corresponding boundary conditions are shown in Fig. 2.

Usually, the FEM requires refined domain mesh to capture the interaction of the matrix and the polygonal fiber in the composite model shown in Fig. 2, while in the BEM, boundary discretization of the fiber and matrix subdomains is separately required and additional equation is needed to establish the connection of the two subdomains. In this study, special polygonal fiber elements based on the fundamental solution approximation of elastic problems are developed to avoid the domain discretization in the fiber region. This procedure is mathematically described in the following section.

3. Basic Formulations and Special Polygonal Fiber Elements

3.1. *Basic formulations*

For the fiber-reinforced composite under consideration, the weak-form of integral formulation in a particular hybrid element e, either general element or special element as shown in Fig. 3, can be written as follows [Qin (2003)]

$$\Pi_{\mathrm{me}} = \frac{1}{2}\int_{\Omega_e} \boldsymbol{\sigma}^T \boldsymbol{\varepsilon} d\Omega - \int_{\Gamma_e^s} \bar{\mathbf{s}}^T \tilde{\mathbf{u}} d\Gamma + \int_{\Gamma_e} \mathbf{s}^T (\tilde{\mathbf{u}} - \mathbf{u}) d\Gamma, \tag{2}$$

where $\boldsymbol{\sigma} = \{\sigma_{11} \quad \sigma_{22} \quad \sigma_{12}\}^T$, $\boldsymbol{\varepsilon} = \{\varepsilon_{11} \quad \varepsilon_{22} \quad \gamma_{12}\}^T$ and $\mathbf{u} = \{u_1 \quad u_2\}^T$ are respectively stress, strain and displacement fields in the element domain Ω_e, $\tilde{\mathbf{u}} = \{\tilde{u}_1 \quad \tilde{u}_2\}^T$ is the compatible displacement field defined on the boundary

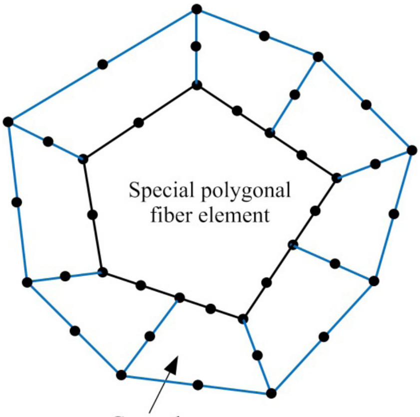

Fig. 3. Typical hybrid finite elements including special polygonal element and general quadrilateral elements.

$\partial\Omega_e = \Gamma_e$ with an outward normal $\mathbf{n} = \{n_1 \quad n_2\}^T$, $\mathbf{s} = \mathbf{A}\boldsymbol{\sigma}$ is the traction field with

$$\mathbf{A} = \begin{bmatrix} n_1 & 0 & n_2 \\ 0 & n_2 & n_1 \end{bmatrix} \tag{3}$$

and $\bar{\mathbf{s}}$ denotes the specified traction distribution on the boundary Γ_e^s.

Provided that the internal displacement and stress fields satisfy the governing equation in the element domain, applying the Gaussian divergence theorem to the functional Π_{me} yields

$$\Pi_{\mathrm{me}} = -\frac{1}{2}\int_{\Gamma_e} \mathbf{u}^T \mathbf{s} d\Gamma - \int_{\Gamma_e^s} \bar{\mathbf{s}}^T \tilde{\mathbf{u}} d\Gamma + \int_{\Gamma_e} \mathbf{s}^T \tilde{\mathbf{u}} d\Gamma. \tag{4}$$

In the application of variational principle, the displacement field in the interior of the element is approximated by a linear combination of fundamental solutions centered at series of source points $\mathbf{x}^s$ locating on the pseudo boundary similar to the element boundary Γ_e, that is,

$$\mathbf{u} = \mathbf{N}\mathbf{c}_e, \tag{5}$$

where $\mathbf{c}_e = \{c_1^1 \quad c_1^2 \mid \cdots \mid c_M^1 \quad c_M^2\}^T$ is a coefficient vector consisting of unknown source intensity at M source points locating on the pseudo boundary outside the element domain [Wang and Qin (2008, 2009)], and $\mathbf{N}$ is a coefficient matrix consisting of the fundamental solution $u_{li}^*(\mathbf{x}, \mathbf{x}_k^s)$:

$$\mathbf{N} = \left[\begin{array}{cc|c|cc} u_{11}^*(\mathbf{x}, \mathbf{x}_1^s) & u_{21}^*(\mathbf{x}, \mathbf{x}_1^s) & \cdots & u_{11}^*(\mathbf{x}, \mathbf{x}_M^s) & u_{21}^*(\mathbf{x}, \mathbf{x}_M^s) \\ & & & & \\ u_{12}^*(\mathbf{x}, \mathbf{x}_1^s) & u_{22}^*(\mathbf{x}, \mathbf{x}_1^s) & \cdots & u_{12}^*(\mathbf{x}, \mathbf{x}_M^s) & u_{22}^*(\mathbf{x}, \mathbf{x}_M^s) \end{array}\right]. \tag{6}$$

In Eq. (5), the displacement fundamental solutions u^*_{li} and the corresponding stress and traction fundamental solutions σ^*_{lij}, s^*_{li} for the plane strain problems are respectively given by [Brebbia and Dominguez (1992)]

$$\begin{aligned}
u^*_{li}(\mathbf{x},\mathbf{x}^s) &= \frac{1}{8\pi G(1-\nu)}\left[(3-4\nu)\delta_{li}\ln\frac{1}{r}+r_{,l}r_{,i}\right],\\
\sigma^*_{lij}(\mathbf{x},\mathbf{x}^s) &= \frac{1}{4\pi(1-\nu)r}[(1-2\nu)(r_{,l}\delta_{ij}-r_{,j}\delta_{il}-r_{,i}\delta_{jl})-2r_{,i}r_{,j}r_{,l}],\\
s^*_{li} = \sigma^*_{lij}n_j &= \frac{-1}{4\pi(1-\nu)r}\left\{[(1-2\nu)\delta_{li}+2r_{,l}r_{,i}]\frac{\partial r}{\partial n}-(1-2\nu)(r_{,l}n_i-r_{,i}n_l)\right\}
\end{aligned} \tag{7}$$

in which δ_{ij} is the Kronecker delta and

$$r=\sqrt{r_ir_i}, \quad r_i = x_i - x^s_i, \quad r_{,i} = \partial r/\partial x_i = r_i/r. \tag{8}$$

Subsequently, according to the strain–displacement equations and the stress–strain relationship, the corresponding stress components and tract components are expressed as

$$\boldsymbol{\sigma} = \mathbf{T}\mathbf{c}_e \tag{9}$$

and

$$\mathbf{s} = \mathbf{Q}\mathbf{c}_e \tag{10}$$

with

$$\mathbf{T} = \left[\begin{array}{cc:c:cc}
\sigma^*_{111}(\mathbf{x},\mathbf{x}^s_1) & \sigma^*_{211}(\mathbf{x},\mathbf{x}^s_1) & \cdots & \sigma^*_{111}(\mathbf{x},\mathbf{x}^s_M) & \sigma^*_{211}(\mathbf{x},\mathbf{x}^s_M)\\
\sigma^*_{122}(\mathbf{x},\mathbf{x}^s_1) & \sigma^*_{222}(\mathbf{x},\mathbf{x}^s_1) & \cdots & \sigma^*_{122}(\mathbf{x},\mathbf{x}^s_M) & \sigma^*_{222}(\mathbf{x},\mathbf{x}^s_M)\\
\sigma^*_{112}(\mathbf{x},\mathbf{x}^s_1) & \sigma^*_{212}(\mathbf{x},\mathbf{x}^s_1) & \cdots & \sigma^*_{112}(\mathbf{x},\mathbf{x}^s_M) & \sigma^*_{212}(\mathbf{x},\mathbf{x}^s_M)
\end{array}\right] \tag{11}$$

and

$$\mathbf{Q} = \left[\begin{array}{cc:c:cc}
s^*_{11}(\mathbf{x},\mathbf{x}^s_1) & s^*_{21}(\mathbf{x},\mathbf{x}^s_1) & \cdots & s^*_{11}(\mathbf{x},\mathbf{x}^s_M) & s^*_{21}(\mathbf{x},\mathbf{x}^s_M)\\
s^*_{12}(\mathbf{x},\mathbf{x}^s_1) & s^*_{22}(\mathbf{x},\mathbf{x}^s_1) & \cdots & s^*_{12}(\mathbf{x},\mathbf{x}^s_M) & s^*_{22}(\mathbf{x},\mathbf{x}^s_M)
\end{array}\right]. \tag{12}$$

It is obvious that the induced stress fields also analytically satisfy the equilibrium within the element, due to the characteristic of fundamental solutions.

In order to enforce the conformity of the displacement field on the common interface of adjacent elements, the element boundary displacement field $\tilde{\mathbf{u}}$ can be interpolated from the generalized nodal displacement $\mathbf{d}_e$ in the form

$$\tilde{\mathbf{u}} = \tilde{\mathbf{N}}\mathbf{d}_e, \tag{13}$$

where $\tilde{\mathbf{N}}$ denotes the matrix consisting of shape functions widely used in the standard FEM and BEM. For example, if the displacements on an element boundary is interpolated by using quadratic shape functions, then for the ith element side consisting of nodes i, j, k, we have

$$\tilde{\mathbf{u}} = \begin{bmatrix} -\frac{\xi(1-\xi)}{2} & 0 & 1-\xi^2 & 0 & \frac{\xi(1+\xi)}{2} & 0 \\ 0 & -\frac{\xi(1-\xi)}{2} & 0 & 1-\xi^2 & 0 & \frac{\xi(1+\xi)}{2} \end{bmatrix} \begin{Bmatrix} d_{2i-1} \\ d_{2i} \\ d_{2j-1} \\ d_{2j} \\ d_{2k-1} \\ d_{2k} \end{Bmatrix}, \tag{14}$$

where ξ is the local natural coordinate of the edge under consideration.

The substitution of Eqs. (5), (10) and (13) into the functional (4) gives

$$\Pi_{\mathrm{me}} = -\frac{1}{2}\mathbf{c}_e^T \mathbf{H}_e \mathbf{c}_e - \mathbf{d}_e^T \mathbf{g}_e + \mathbf{c}_e^T \mathbf{G}_e \mathbf{d}_e \tag{15}$$

which includes boundary integrals only, and

$$\mathbf{H}_e = \int_{\Gamma_e} \mathbf{Q}^T \mathbf{N} d\Gamma, \quad \mathbf{G}_e = \int_{\Gamma_e} \mathbf{Q}^T \tilde{\mathbf{N}} d\Gamma, \quad \mathbf{g}_e = \int_{\Gamma_e^s} \tilde{\mathbf{N}}^T \bar{\mathbf{s}} d\Gamma. \tag{16}$$

The stationarity of Π_{me} with respect to the displacement coefficient $\mathbf{c}_e$ and nodal displacement $\mathbf{d}_e$ yields the following optional relationship between $\mathbf{c}_e$ and $\mathbf{d}_e$

$$\mathbf{c}_e = \mathbf{H}_e^{-1} \mathbf{G}_e \mathbf{d}_e \tag{17}$$

and the element displacement–load equation given by

$$\mathbf{K}_e \mathbf{d}_e = \mathbf{g}_e \tag{18}$$

with the symmetric element stiffness matrix

$$\mathbf{K}_e = \mathbf{G}_e^{\mathbf{T}} \mathbf{H}_e^{-1} \mathbf{G}_e. \tag{19}$$

3.2. *Special polygonal fiber elements*

It is known that an element with arbitrary number of sides is difficult to construct using the conventional finite element procedure, thus in the conventional FEM, just triangular and quadrilateral elements are used for plane problems. In contrast, with the hybrid formulation described above, it is easy to construct n-sided polygonal elements with more nodes and edges than the conventional finite elements, due to the fact of the independence of interior displacement and boundary displacement fields. More importantly, because the interior approximating displacement and stress fields analytically satisfy the elastic governing equations within the element domain, all integrals are evaluated along the element boundary only. Thus, it is possible to design the super elements with multiple element edges to achieve significant mesh reduction in the inclusion region.

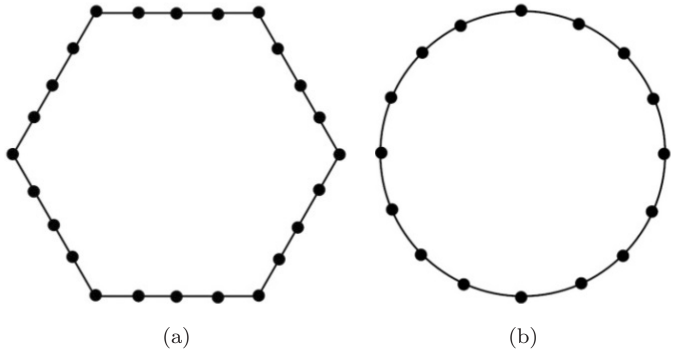

Fig. 4. Configuration of special polygonal fiber elements for the (a) hexagonal and (b) circular fibers.

Although arbitrarily shaped fibers such as circular, triangular, square or hexagonal ones can be studied theoretically using the present hybrid finite element formulation, in the paper, just the hexagonal and circular fibers are investigated for the sake of simplicity. According to the theory of the present algorithm, the hybrid special polygonal fiber elements with multi-edges can be constructed to model the hexagonal and circular fibers, as displayed in Fig. 4, in which special polygonal elements have 24 and 16 nodes, respectively. Besides, the general hybrid finite element with four edges and eight nodes [Wang and Qin (2011a)] are used to model the matrix to provide flexible mesh strategy implemented by the commercial finite element software like ABAQUS.

4. Numerical Examples

The matrix material of the composite with periodic hexagonal and circular fibers is considered to be isotropic and homogeneous, and the elastic modulus and Poisson's ratio of the medium are respectively taken as $E^{(\mathrm{M})} = 1$, $v^{(\mathrm{M})} = 0.3$. The isotropic and homogeneous elastic fiber is assumed to have same Poisson's ratio as the one of matrix, and its elastic modulus is assumed to be $E^{(\mathrm{I})}/E^{(\mathrm{M})} = 10$. For the sake of convenience, the geometry size of the unit cell is taken as h/l =1 with the assumption of h= 0.5.

Besides, in order to analyze the dependence of elastic properties of fiber composites on the fiber concentration, the unit cell shown in Fig. 2 is analyzed by the proposed special polygonal fiber element, and two different fiber concentrations are taken into consideration: 10% and 30% for representing respectively moderate and high fiber volume fraction.

4.1. *Hexagonal fiber*

For the hexagonal fiber, a moderate volume concentration 10% is firstly considered. In the analysis, the side length of the hexagonal fiber is set to be 0.1962.

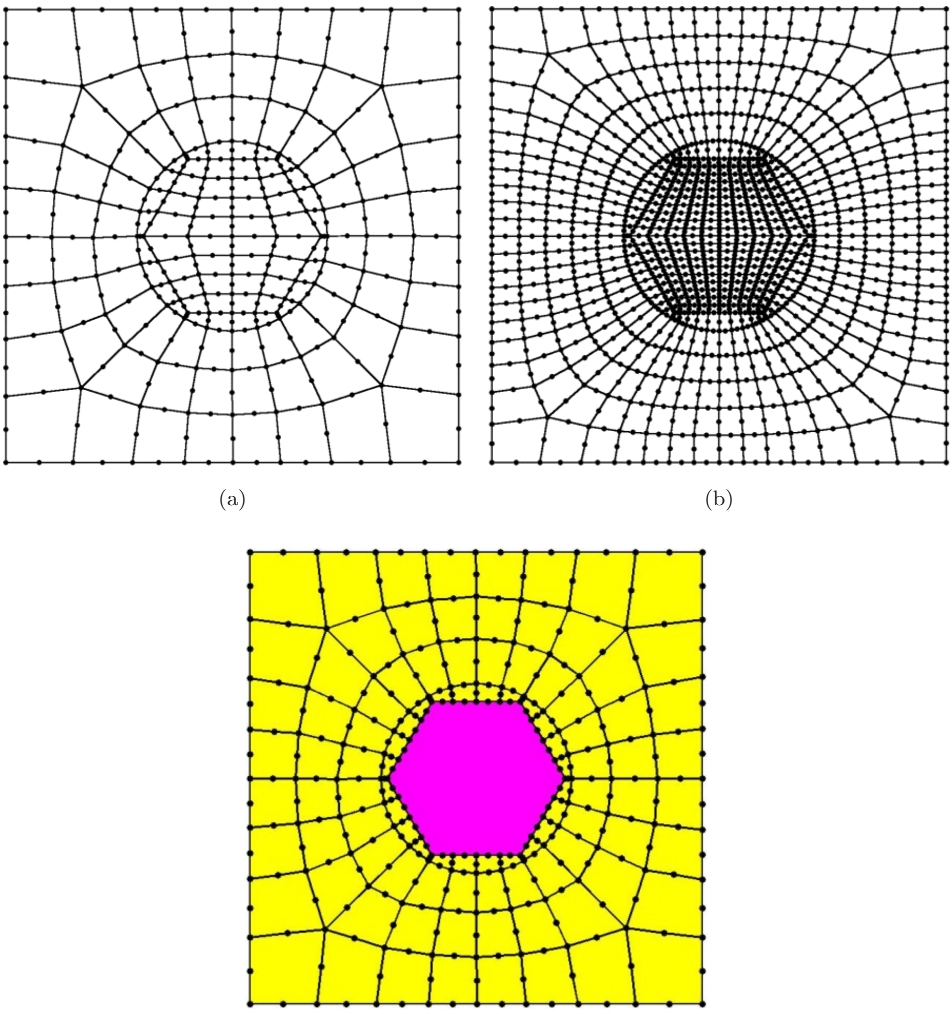

(a) (b) (c)

Fig. 5. Illustration of mesh divisions in the unit cell with hexagonal fiber by ABAQUS and HFS-FEM for the case of $\alpha = 10\%$. (a) Coarse mesh by ABAQUS, (b) Refined mesh by ABAQUS and (c) Mesh by HFS-FEM.

Figure 5 displays three mesh strategies respectively produced by ABAQUS and HFS-FEM in the unit cell with a hexagonal fiber. In order to show the advantage of the present special polygonal fiber elements, we keep the mesh to be the same in the matrix region for both ABAQUS with coarse mesh (named as ABAQUS1 for convenience) and HFS-FEM, while in the fiber region, the mesh strategy is distinctively different. For the mesh discretization generated by ABAQUS, some typical quadratic isoparametric elements are produced to discretize the fiber domain in meeting element connection and keeping reasonable the aspect ratio of element, while in the HFS-FEM, only one special polygonal fiber element is employed to model the fiber domain and no any nodes are put inside the fiber. In addition, the refined mesh by ABAQUS (named as ABAQUS2) is generated to give more accurate results than the coarse mesh. In ABAQUS, the total number of elements is 132 with 429 nodes (coarse mesh) and 564 elements with 1761 nodes (refined mesh). In contrast, the total number of elements in the present approach is just 101 including a special element with 24 edges and 48 nodes, and the total number of nodes reduces to 356, which has 17% decrease in comparison with that of coarse mesh in ABAQUS while the same mesh division is used outside the inclusion. It is obvious that the mesh reduction is achieved by the present special polygonal fiber element. Numerical results on the variation of traction components along the outer boundary of the unit cell are plotted in Fig. 6, from which one can observe that there is a good agreement between the numerical results of HFS-FEM and those of ABAQUS. It is necessary to point out that the boundary length in Fig. 6 and next figures is measured in anti-clockwise direction by starting from the lower left point in Fig. 2. Moreover, from the local enlargement in Fig. 6, it is seen that better accuracy can be achieved by the present special polygonal fiber element than the elements in ABAQUS with coarse mesh. So, the accuracy and efficiency of the present special polygonal fiber element is demonstrated for the analysis of composite embedded with hexagonal fibers.

Besides, to illustrate the convergence of the present polygonal element, three element meshes (the solution domain is divided with 24, 36, 48 nodes, respectively) are used. The results of average value of the traction component t_1 which is evaluated by trapezoidal integration are tabulated in Table 1, from which it is found that the accuracy increases along with an increase in the number of nodes of the polygonal

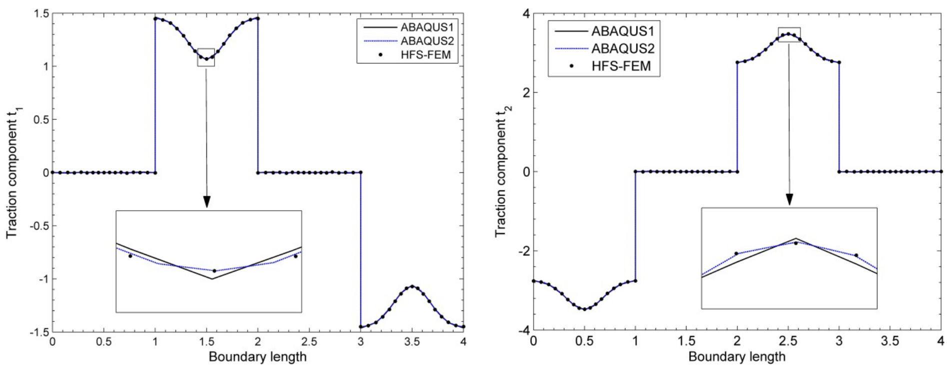

(a) (b)

Fig. 6. Traction distributions along the outer boundary of the unit cell with hexagonal fiber for the case of $\alpha = 10\%$. (a) Traction component t_1 and (b) traction component t_2.

Table 1. Convergent demonstration for three different special elements.

Number of edges	Number of nodes	Average value of t_1	Percentage error (%)
12	24	1.2893	0.1
18	36	1.2882	0.02
24	48	1.2880	—

element. In Table 1, the percentage error is evaluated by taking the average value from the mesh with 48-node as reference.

Next, a composite with a larger volume concentration of 30% of the hexagonal fiber is considered. In this case, the side length of the hexagonal fiber is assumed to be 0.398. Due to the volume increase of the hexagonal fiber, ABAQUS requires proper partition in the hexagonal domain to produce relatively regular mesh in the unit cell. At the same time, more elements are needed to simulate strong interaction of the hexagonal fiber and the cell boundary. In Fig. 7(a), a refined mesh including 910 elements and 2825 nodes is used in ABAQUS to produce stable and accurate numerical results, for the purpose of comparison. In contrast, the HFS-FEM employs fewer elements including 114 general hybrid finite elements and one special polygonal fiber element only, in which 30 edges and 60 nodes are involved. Figure 8 plots the variation of tractions along the outer boundary of unit cell and it is evident that the use of special hexagonal fiber element can produce almost same accuracy as that in the ABAQUS with more elements, but the computing size is greatly decreased by the present algorithm. Also, by comparison of the results in Figs. 6 and 8, it is found that an increase in the volume fraction of hexagonal fiber

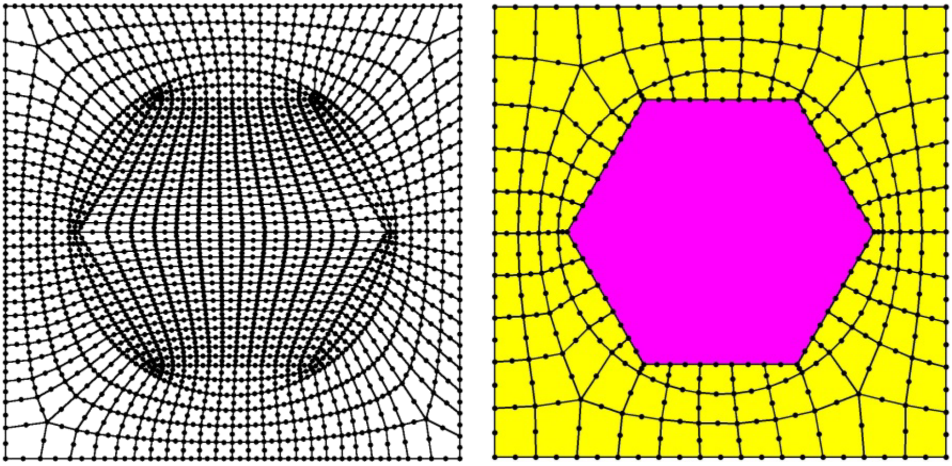

(a) (b)

Fig. 7. Illustration of mesh divisions in the unit cell with hexagonal fiber by ABAQUS and HFS-FEM for the case of $\alpha = 30\%$. (a) Refined mesh by ABAQUS and (b) mesh by HFS-FEM.

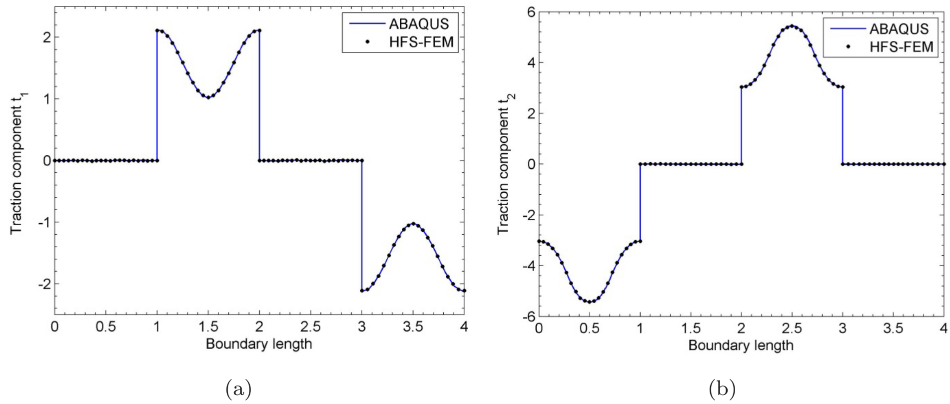

Fig. 8. Traction distributions along the outer boundary of the unit cell with hexagonal fiber for the case of $\alpha = 30\%$. (a) Traction component t_1 and (b) traction component t_2.

causes dramatic increase of traction forces. This will induce larger overall elastic properties of composites, according to Dong's formulation [2006].

4.2. *Circular fiber*

When the number of sides of the polygonal fiber increases to infinity, the polygonal fiber becomes the circular fiber. In this section, the mechanical response of the composite with a circular inclusion is investigated.

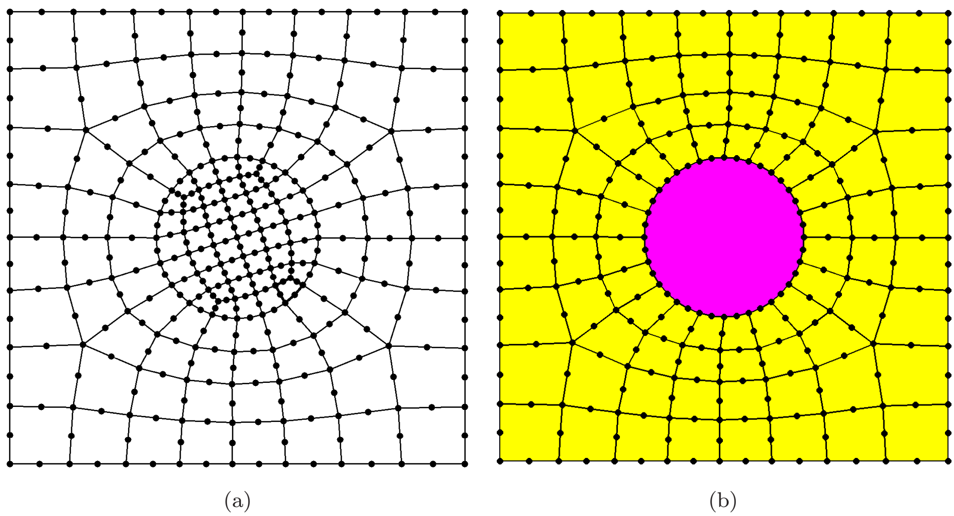

Fig. 9. Illustration of mesh divisions in the unit cell with circular fiber by ABAQUS and HFS-FEM for the case of $\alpha = 10\%$. (a) Refined mesh by ABAQUS and (b) mesh by HFS-FEM.

For a moderate fiber volume fraction, i.e., $\alpha = 10\%$, a typical mesh division is shown in Fig. 9. For the sake of comparison, we use the same mesh to model the matrix for both ABAQUS and HFS-FEM, while in the inclusion, the mesh strategy is different. For the mesh discretization generated by ABAQUS, some typical quadratic isoparametric elements are produced to discretize the inclusion domain. The total number of elements in the ABAQUS is 124 elements with 405 nodes. In contrast, a super element with 20 edges is employed in the developed HFS-FEM to model the inclusion and no node is placed inside the inclusion. Thus, the total number of elements in the present HFS-FEM is just 81 and the number of nodes reduces to 292, which deceases in 27.9% compared to that in ABAQUS. It is obvious that the mesh reduction is achieved using the present special polygonal element.

Besides, the variation of traction components along the outer boundary of the unit cell is displayed in Fig. 10, from which a good agreement is observed between the numerical results of HFS-FEM and those of ABAQUS. So, the accuracy and efficiency of the present super hybrid element is demonstrated again for the analysis of periodic composite embedded with circular fibers.

When the volume fraction of the inclusion increases to 30%, for ABAQUS, more elements are required to model the solution domain. As shown in Fig. 11, total 432 quadratic isoparametric quadrilateral elements with 1353 nodes are included in the analysis using ABAQUS. While, for the proposed HFS-FEM, only 77 elements including 284 nodes are used, as displayed in Fig. 11. Figure 12 shows the traction distribution along the outer boundary of the unit cell and a good agreement between the numerical results of HFS-FEM and those of ABAQUS is found again. Moreover, it is seen that traction component for the case of $\alpha = 30\%$ has more dramatic change than that for the case of $\alpha = 10\%$. The main reason is that the interaction between

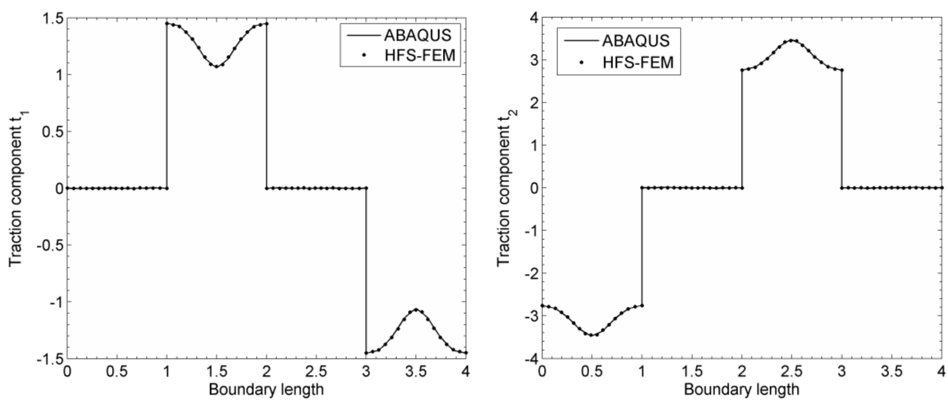

(a) (b)

Fig. 10. Traction distributions along the outer boundary of the unit cell with circular fiber for the case of $\alpha = 10\%$. (a) Traction component t_1 and (b) traction component t_2.

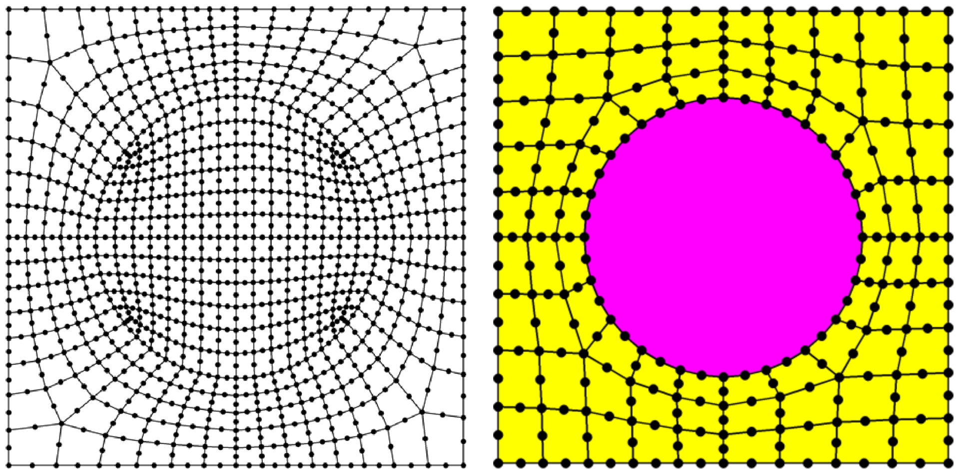

(a) (b)

Fig. 11. Illustration of mesh divisions in the unit cell with circular fiber by (a) ABAQUS and (b) HFS-FEM for the case of $\alpha = 30\%$.

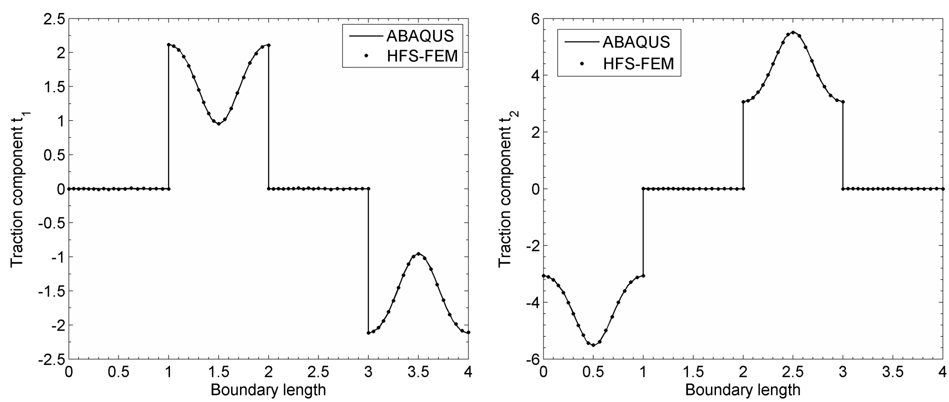

(a) (b)

Fig. 12. Traction distributions along the outer boundary of the unit cell with circular fiber for the case of $\alpha = 30\%$. (a) Traction component t_1 and (b) traction component t_2.

the inclusion and the unit cell boundary becomes strong as the volume fraction of the inclusion increases.

Finally, in order to clearly show the variation of tractions for different fiber types and fiber volume fractions, Figs. 13 and 14 are respectively plotted along the right edge and bottom edge of the unit cell. It is found from these two figures that for the case of 10% fiber volume fraction, both the hexagonal and circular fibers produce almost same traction results. While for the case of 30% fiber volume

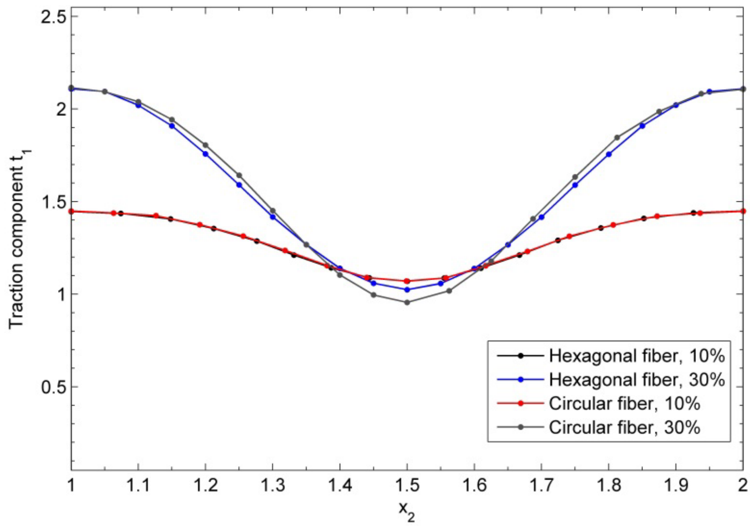

Fig. 13. Traction component t_1 along the right edge of the unit cell.

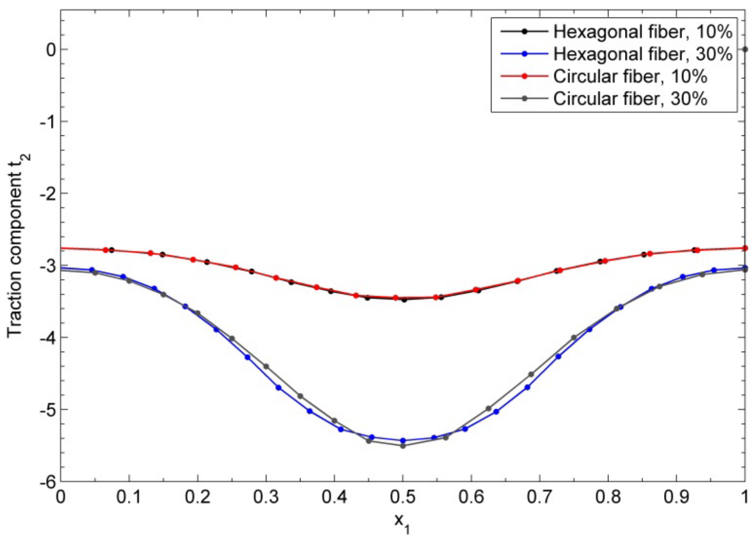

Fig. 14. Traction component t_2 along the bottom edge of the unit cell.

fraction, the hexagonal fiber and the circular fiber induce a significant different traction distributions.

5. Conclusions

The present study proposes a fundamental-solution-based hybrid finite element model for analysing unidirectional fiber reinforced composites including hexagonal and circular fibers. Plane elastic fundamental solutions rather than conventional shape functions are employed to approximate the element interior displacement and stress fields, so that unconventional elements are made due to multiplicity in the number of nodes and edges. By virtue of the property of the present hybrid element, we can construct special polygonal fiber elements with multiple edges and nodes to flexibly model the fiber region for the purpose of mesh reduction and do not need to perform mesh discretization inside the fiber inclusion. The numerical accuracy and efficiency on mesh reduction and convergence of the present technology are illustrated and the numerical results show that there are good agreements of the present results with the results available by ABAQUS. Therefore, the present special polygonal fiber element is promising for solving composite problems with periodic array of polygonal fibers and determining their effective elastic properties.

Acknowledgments

The work described in this paper was partially supported by the National Natural Science Foundation of China (Nos. 11102059, 11372100, 11472099) and the Program for Innovation Talents of Science and Technology in Universities in Henan Province (No. 13HASTIT019).

References

Bonnet, G. [2007] "Effective properties of elastic periodic composite media with fibers," *J. Mech. Phys. Solid* **55**, 881–899.

Brebbia, C. A. and Dominguez, J. [1992] *Boundary Elements: An Introductory Course* (Computational Mechanics Publications, Southampton).

Dong, C. Y. [2006] "Effective elastic properties of doubly periodic array of inclusions of various shapes by the boundary element method," *Int. J. Solid Struct.* **43**, 7919–7938.

Feng, X. Q., Mai, Y. W. and Qin, Q. H. [2003] "A micromechanical model for interpenetrating multiphase composites," *Comput. Mater. Sci.* **28**, 486–493.

Ghosh, S. [2011] *Micromechanical Analysis and Multi-Scale Modeling Using the Voronoi Cell Finite Element Method* (CRC Press, Boca Raton).

Kaminski, M. [1999] "Boundary element method homogenization of the periodic linear elastic fiber composites," *Eng. Anal. Bound. Elem.* **23**, 815–824.

Michel, J., Moulinec, H. and Suquet, P. [1999] "Effective properties of composite materials with periodic microstructure: A computational approach," *Comput. Meth. Appl. Mech. Eng.* **172**, 109–143.

Mogilevskaya, S. G. and Crouch, S. L. [2013] "Combining Maxwell's methodology with the BEM for evaluating the two-dimensional effective properties of composite and micro-cracked materials," *Comput. Mech.* **51**, 377–389.

Qin, Q. H. [2000] *The Trefftz Finite and Boundary Element Method* (WIT Press, Southampton).

Qin, Q. H. [2003] "Variational formulations for TFEM of piezoelectricity," *Int. J. Solid Struct.* **40**, 6335–6346.

Qin, Q. H. and Wang, H. [2008] *Matlab and C Programming for Trefftz Finite Element Methods* (CRC Press, New York).

Qin, Q. H. and Wang, H. [2013] "Special circular hole elements for thermal analysis in cellular solids with multiple circular holes," *Int. J. Comput. Methods* **10**, 1350008.

Qin, Q. H. and Yang, Q. S. [2008] *Macro-Micro Theory on Multifield Coupling Behavior of Heterogeneous Materials* (Higher Education Press and Springer, Berlin).

To, Q. D., Bonnet, G. and To, V. T. [2013] "Closed-form solutions for the effective conductivity of two-phase periodic composites with spherical inclusions," *Proc. Math. Phys. Eng. Sci. A* **469**, 20120339.

Wang, H., Cao, L. L. and Qin, Q. H. [2012] "Hybrid graded element model for nonlinear functionally graded materials," *Mech. Adv. Mater. Struct.* **19**, 590–602.

Wang, H. and Qin, Q. H. [2008] "Meshless approach for thermo-mechanical analysis of functionally graded materials," *Eng. Anal. Bound. Elem.* **32**, 704–712.

Wang, H. and Qin, Q. H. [2009] "Hybrid FEM with fundamental solutions as trial functions for heat conduction simulation," *Acta Mech. Solida Sin.* **22**, 487–498.

Wang, H. and Qin, Q. H. [2011a] "Fundamental-solution-based hybrid FEM for plane elasticity with special elements," *Comput. Mech.* **48**, 515–528.

Wang, H. and Qin, Q. H. [2011b] "Special fiber elements for thermal analysis of fiber-reinforced composites," *Eng. Comput.* **28**, 1079–1097.

Wang, H. and Qin, Q. H. [2012] "Numerical implementation of local effects due to two-dimensional discontinuous loads using special elements based on boundary integrals," *Eng. Anal. Bound. Elem.* **36**, 1733–1745.

Würkner, M., Berger, H. and Gabbert, U. [2011] "On numerical evaluation of effective material properties for composite structures with rhombic fiber arrangements," *Int. J. Eng. Sci.* **49**, 322–332.

Yang, Q. S. and Qin, Q. H. [2004] "Micro-mechanical analysis of composite materials by BEM," *Eng. Anal. Bound. Elem.* **28**, 919–926.

Yu, S. W. and Qin, Q. H. [1996] "Damage analysis of thermopiezoelectric properties: Part II, Effective Crack Model," *Theor. Appl. Fract. Mech.* **25**, 279–288.